Chin. Phys. Lett. **39**, 073201 (2022)

Reconciliation of Theoretical Lifetimes of the $5s5p\,^3P_2^o$ Metastable State for ^{88}Sr with Measurement: The Role of the Blackbody-Radiation-Induced Decay

Benquan Lu(卢本全)[1], Xiaotong Lu(卢晓同)[1], Jiguang Li(李冀光)[2*], and Hong Chang(常宏)[1,3*]

[1]*National Time Service Center, Chinese Academy of Sciences, Xi'an 710600, China*
[2]*Institute of Applied Physics and Computational Mathematics, Beijing 100088, China*
[3]*The University of Chinese Academy of Sciences, Beijing 100088, China*

(Received 7 May 2022; accepted manuscript online 6 June 2022)

We conducted measurement and calculation to resolve the long-standing large discrepancy in the metastable state lifetime for the ^{88}Sr atom between theoretical and experimental results. The present lifetime $\tau = 830^{+600}_{-240}$ s, measured using the magneto-optical trap as a photon amplifier to detect the weak decay events, is approximately 60% larger than the previous experimental value $\tau = 520^{+310}_{-140}$ s. By considering the electron correlation effects in the framework of the multiconfiguration Dirac–Hartree–Fock theory, we obtained a theoretical lifetime of 1079(54) s, which lies in the range of measurements with error bars. Furthermore, we considered the higher-order electron correlation and Breit interaction to control the uncertainty of the theoretical calculation. The significant improvement in the agreement between calculations and measurements is attributed to the updated blackbody radiation-induced decay rate.

DOI: 10.1088/0256-307X/39/7/073201

In alkaline-earth-metal-like atoms, lifetimes of levels in the first excited configuration $nsnp$ are of great importance in various applications. For example, the $nsnp\ ^3P_1^o$ state can be used to investigate the continuous laser cooling of atoms down to the ultracold temperature[1−4] and the ultracold atomic collisions.[5] Moreover, the $^1S_0$–$^3P_0^o$ transition has been selected as a frequency reference for the optical clock.[6−11] Recently, the optical lattice clock based on strontium atoms shows an accuracy of 10^{-18}, and its stability reaches the level of 10^{-19}.[8,9] Traditionally, the improvement in the stability of optical clocks is to increase the length of the ultra-low expansion cavity used as the local oscillator; however, it depends on the materials of the cavity and the techniques for reducing the frequency noise.[12] A new method was proposed by applying the $5s5p\,^3P_2^o$–$5s4d\,^3D_3$ cyclic transition to generate a metastable magneto-optical trap (MOT) instead of the common red MOT based on the $5s^2\,^1S_0$–$5s5p\,^3P_1^o$ transition. This new type of MOT can increase the captured atom number and reduce the cooling time.[4,13,14] Additionally, the $^1S_0$–$^3P_2^o$ transition is employed to create quantum degenerate gases.[15] The anisotropic collisions,[16,17] quantum simulation,[18] and quantum computation[19] can be investigated using the trapped alkaline-earth-metal-like atoms in the $^3P_2^o$ state. However, most of these applications require the accurate determination of the lifetime of the $^3P_2^o$ state.

Derevianko[20] presented a theoretical lifetime of the $^3P_2^o$ state for ^{88}Sr atoms for the first time. This value $\tau = 1048$ s was obtained using the relativistic valence configuration interaction (CI) method coupled with random-phase approximation. Liu *et al.*[21] performed another calculation using the multiconfiguration Dirac–Fock method. Their result $\tau = 1071$ s is consistent with that of Derevianko. However, these two theoretical predictions are about two times larger than the experimental value $\tau = 520^{+310}_{-140}$ s by Yasuda and Katori[22] using the fluorescence decay of the ^{88}Sr atoms trapped in an MOT.

In this study, we remeasured the lifetime of the $^3P_2^o$ state for ^{88}Sr using MOT as a photon amplifier to detect the decay events. Our result is approximately 60% larger than the previous measurement by Yasuda and Katori.[22] This considerable correction arises from the more accurate black-body-radiation (BBR) induced decay rate adopted to deduce the lifetime. We also performed calculations on rates of the primary decay channels from the $^3P_2^o$ state, i.e., the $^1S_0$–$^3P_2^o$ magnetic quadrupole (M2) and $^3P_1^o$–$^3P_2^o$ magnetic dipole (M1) transitions based on the multiconfiguration Dirac–Hartree–Fock (MCDHF) method. On the basis of these values, the lifetime of the $^3P_2^o$ state was derived from $\tau = \frac{1}{A(\mathrm{M2})+A(\mathrm{M1})}$. Our theoretical result is consistent with the previous calculations.

*Corresponding authors. Email: li_jiguang@iapcm.ac.cn; changhong@ntsc.ac.cn
© 2022 Chinese Physical Society and IOP Publishing Ltd

Therefore, the updated BBR-induced decay rate reconciles the long-standing inconsistency in the lifetime of $^3P_2^o$ state for ^{88}Sr between theoretical and experimental values.

The nuclear spin I of bosonic isotopes of Sr equals zero; thus, they lack a hyperfine structure. Figure 1(a) shows the energy levels for ^{88}Sr. From the $^3P_2^o$ state, the $^1S_0$–$^3P_2^o$ M2 and $^3P_1^o$–$^3P_2^o$ M1 transitions are the primary decay channels; they determine the lifetime of the $^3P_2^o$ metastable state. According to the estimate, 99.9% of the atoms populated on the $^3P_2^o$ state can be transferred to the ground state since atoms decayed to the $^3P_1^o$ state can further decay to the ground state in 22 μs.[23] Therefore, we can adopt the ground state population to detect the depopulation from the $^3P_2^o$ state.

Figure 1(b) shows the schematic configuration of the experimental apparatus. After passing through the collimator and Zeeman slower, the strontium atoms ejected from the oven are trapped by the MOT operating on the $^1S_0$–$^1P_1^o$ transition. More details of laser cooling and trapping on the Sr atoms were described in Ref. [24]. The $^1S_0$–$^1P_1^o$ transition is not a perfectly closed cyclic transition as, approximately, one in every 10^5 scattered photons makes some atoms shelved into the $5s5p\,^3P_2^o$ metastable state. The atoms in the $^3P_2^o$ state could be trapped by the quadrupole magnetic field formed through the anti-Helmholtz coils with a gradient of about 50 G/cm along its axis of symmetry. The repumping lasers at $\lambda = 679$ nm and $\lambda = 707$ nm are applied to transfer the metastable atoms back to the ground state.

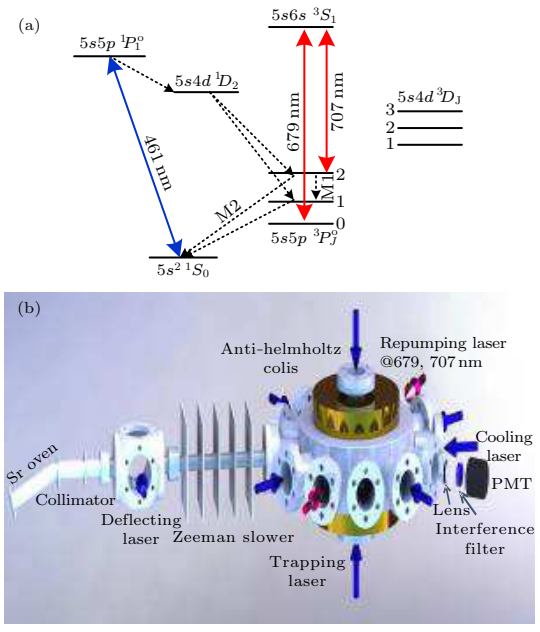

Fig. 1. (a) Relevant energy levels of ^{88}Sr. (b) Schematic configuration of the experimental apparatus.

The change in the atom number in the blue MOT[22] is given as follows:

$$\frac{d}{dt}N_s(t) = -(\gamma_p + \Gamma_c)N_s(t) + (\gamma_r + \Gamma_q)N_p(t), \quad (1)$$

where $N_s(t)$ and $N_p(t)$ are the populations of atoms in the ground and metastable states, respectively. The atoms in the ground state can be collisionally lost with a rate of $\Gamma_c < (10\,\mathrm{s})^{-1}$ or leaked out of the cyclic transition with a rate $\gamma_p \approx (24\,\mathrm{ms})^{-1}$ via the $5s4d\,^1D_2$ state. The ground state population is supplemented from the $^3P_2^o$ state with either radiative decay (γ_r) or collisional quench (Γ_q). In the magnetic trap, the collisional loss rate Γ_m is the dominant decay channel; however, it is much smaller than γ_p. Therefore, the ground state population $N_s(t)$ adiabatically follows that of the metastable state. In the time scale $t \gg \gamma_p^{-1}$, the evolution of the ground state population is given by

$$N_s(t) = \frac{\gamma_r + \Gamma_q}{\gamma_p + \Gamma_c}N_p(t). \quad (2)$$

Assuming that $\Gamma_c \ll \gamma_p$ and $\Gamma_q \ll \gamma_r$ hold, we can neglect the two collisional losses in Eq. (2). Therefore, the decay rate from the $^3P_2^o$ state could be obtained as $\gamma_r = [N_s(t)/N_p(t)] \times \gamma_p$. The number of atoms in the ground state $N_s(t)$ could be obtained by observing the fluorescence signal of the MOT, $I_s(t) = \eta N_s(t)$, where η represents the photon-counting rate per atom trapped in the MOT. Similarly, the metastable state population $N_p(t)$ could be determined by repumping the atoms to the ground state and recording the MOT fluorescence intensity as $I_p(t) = \eta N_p(t)$. The ratio of $N_s(t)/N_p(t) = I_s(t)/I_p(t)$ could be accurately obtained regardless of the coefficient η. Meanwhile, the value of γ_p could be obtained by exponentially fitting the decay of the MOT fluorescence intensity.

The experimental cycle begins by loading the magnetic trap for 1000 ms to trap enough atoms. The trapping lasers, Zeeman slower, and cooling laser were turned off. A deflecting laser is operated at $t = 0$ ms with a blue detuning of 20 MHz to the $^1S_0$–$^1P_1^o$ transition. The efficiency of the deflecting laser was measured to be 90%. Then, we waited for 200 ms to ensure only the magnetically trapped metastable atoms remained in the trap region. At this time ($t = 0$ s), the trapping lasers were turned on again to capture atoms that radiatively decayed from the $^3P_2^o$ state. The fluorescence intensity was recorded using a photomultiplier tube (PMT). The MOT fluorescence was collected using a lens with a solid angle of 0.0187. An interference filter was placed in front of the PMT to block, except for the 461 nm light. At $t = 700$ ms, the repumping lasers were turned on with a duration of 10 ms to transfer the metastable state atoms into the ground state. We determined the value of $I_p(t = 700\,\mathrm{ms})$ by taking the maximum MOT fluorescence intensity.

Figure 2(a) shows the time-resolved fluorescence signal from $t = 0$ ms to $t = 1700$ ms (stage A). To cancel the influences of residual atoms from the Sr oven and other possible noises, the trapping lasers and magnetic field were turned off at $t = 1700$ ms to ensure that all atoms diffused out of the trap region, and 200 ms later, the same experimental procedure was conducted. Figure 2(a) also shows the background signal (stage B). Figure 2(b) shows an average of over 200 measurements of the background-corrected fluorescence signal. The number of atoms in the ground state at $t = 700$ ms was determined by exponentially extrapolating the entire decay curve $I_s(0 < t < 700\,\text{ms})$ of the MOT fluorescence. The fluorescence decay in $0 < t < 700$ ms was primarily caused by the collisional atom lost in the magnetic trap with the decay rate $\Gamma_m \approx (16.7\,\text{s})^{-1}$ at the background gas pressure of 2×10^{-11} torr. After transferring the atoms populated in the metastable state into the ground state at $t = 700$ ms, the MOT fluorescence intensity increased and obtained its maximum at $t = 710$ ms, as presented in the inset of the figure. Then, the signal decayed double exponentially, including the MOT decay γ_p owing to the branching loss and collisional decay Γ_m of the metastable atoms recaptured in the magnetic field trap. The value of γ_p was determined to be $(24.1\,\text{ms})^{-1}$ by exponential fitting the MOT decay since it is more than 400 times larger than Γ_m. Subsequently, the radiative decay rate from the $^3P_2^o$ state was determined to be $\gamma_r = (8.6\pm0.5)\times10^{-3}\,\text{s}^{-1}$; here, the error was the statistical 1σ standard deviation.

In Ref. [22], Yasuda and Katori demonstrated that the BBR field could transfer the atoms populated in the $^3P_2^o$ state to the short-lived $^3P_1^o$ state via the $5s4d\,^3D$ state, which significantly shortens the measured lifetime of the $^3P_2^o$ state. The radiative decay rate (γ_0) from the $^3P_2^o$ metastable state could be determined as the difference between the measurement $\gamma_r(T)$ and the BBR-induced decay rate $\gamma_B(T)$. In this work, we measured the value of γ_r at room temperature. By solving the coupled rate equations, the steady-state value of the BBR-induced decay rate $\gamma_B(T)$ could be expressed as[22,25]

$$\gamma_B(T) = \frac{7}{36}\gamma_D \times \bar{n}(T). \tag{3}$$

Here, $\bar{n}(T) = \{\exp(hc/k_BT\lambda) - 1\}^{-1}$ represents the BBR photon occupation number at temperature T with the wavelength $\lambda \approx 3.01\,\mu$m corresponding to the $^3P_2^o$–^3D transition, and γ_D is the radiative decay rate of the $5s4d\,^3D$ state. A value of $\gamma_D^{-1} = 2.9 \pm 0.2\,\mu$s[26] for the radiative lifetime of the ^3D state was used in Ref. [22], resulting in a measured lifetime of 520^{+310}_{-140} s for the $^3P_2^o$ state. However, the lifetime of the ^3D state was later revised to $\gamma_D^{-1} = 2.522 \pm 0.028\,\mu$s. This value is given by Safronova *et al.*[25] using the CI + all-order method with much small uncertainty. This value was determined by Redondo *et al.*[27] studying the evolution of the low-lying excited states of strontium atom and Nicholson *et al.*[28] observing the count of photons decaying from the $^3P_1^o$ state. Furthermore, we modeled the vacuum chamber and simulated the temperature distribution at the center of the MOT using the finite element method to determine the ambient temperature of the atoms. The average ambient temperature of the atoms under the condition of thermal steady state is 294.95 ± 0.2 K. Therefore, the BBR-induced decay rate is obtained to be $\gamma_B(T = 295.95\,\text{K}) = (7.46 \pm 0.08) \times 10^{-3}\,\text{s}^{-1}$.

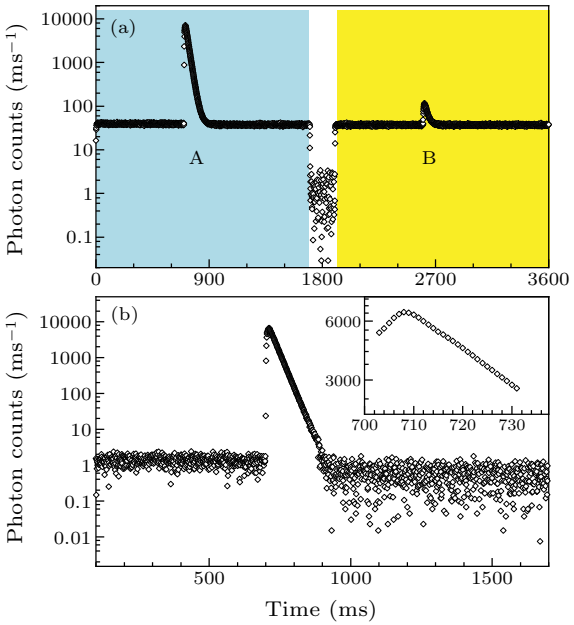

Fig. 2. The time-resolved fluorescence signal. (a) A typical data recording cycle of the MOT fluorescence. Stage A indicates the experimental data with the noise and signal. Stage B represents the noise. (b) The background-corrected fluorescence intensity averaged over 200 measurements. The fluorescence signal at $0 < t < 700$ ms indicates the photons scattered by the recaptured atoms in the ground state by repumping lasers at $\lambda = 679$ nm and $\lambda = 707$ nm. At $t = 700$ ms, the $^3P_2^o$ metastable state population is pumped to the ground state. The peak intensity indicates the number of atoms in the metastable state. The inset shows the zoom-in figure around the peak. The fluorescence intensity reaches its maximum at approximately 10 ms.

We also evaluated other possible factors that may affect the measurement. First, the collisional loss would occur during the transfer of the atoms from the $^3P_2^o$ state to the ground state by the repumping lasers. As shown in Fig. 2(b), the transferring period is about $\tau_p = 10$ ms, and the fraction of the collisional loss is estimated to be $1 - \exp(-\Gamma_m\tau_p) \approx 10^{-4}$. Second, we increased the temperature of the oven and measured the radiative decay rate to consider the thermal radiation from the Sr oven. Consequently, we obtained that the thermal radiation of the oven has a negligible

effect on the decay rate.

According to the aforementioned analyses, we derived the $^3P_2^o$ metastable state decay rate $\gamma_0 = (1.2 \pm 0.5) \times 10^{-3}\,\mathrm{s}^{-1}$. The uncertainty of the radiative lifetime of the ^3D state brings an error of $0.1 \times 10^{-3}\,\mathrm{s}^{-1}$ for the BBR-induced decay rate $\gamma_\mathrm{B}(T)$. The statistical error of the measurement is $0.5 \times 10^{-3}\,\mathrm{s}^{-1}$. Finally, the natural lifetime of the $^3P_2^o$ metastable state for ^{88}Sr is obtained to be 830^{+600}_{-240} s, which is approximately 60% larger than the result 520^{+310}_{-140} s in Ref. [22].

Meanwhile, the atomic structure calculation was conducted using the MCDHF and relativistic configuration interaction (RCI) methods.[29,30] The core idea of these two methods is to express an atomic state function $\Psi(\Gamma PJM_J)$ as a linear combination of configuration state functions (CSFs) $\Phi(\gamma PJM_J)$ with the same parity P, total angular momentum J and its component along z direction M_J, i.e.,

$$\Psi(\Gamma PJM_J) = \sum_i^N c_i \Phi_i(\gamma_i PJM_J). \tag{4}$$

Here, c_i stands for the mixing coefficient, and γ represents the other quantum numbers to uniquely define the state. The CSFs are constructed as linear combinations of Slater determinants, each of which is a product of one-electron Dirac orbitals. In the MCDHF method, the mixing coefficients c_i and the radial functions are simultaneously optimized in the self-consistent field procedure, whereas for RCI, only mixing coefficients are variable. In this study, the Breit interaction in the low-frequency approximation,

$$B_{ij} = -\frac{1}{2r_{ij}}\left[\boldsymbol{\alpha}_i \cdot \boldsymbol{\alpha}_j + \frac{(\boldsymbol{\alpha}_i \cdot r_{ij})(\boldsymbol{\alpha}_j \cdot r_{ij})}{r_{ij}^2}\right], \tag{5}$$

is considered in the RCI computation.

The transition rate can be evaluated in terms of line strengths,[31] i.e.,

$$A_{ki} = \frac{2.69735 \times 10^{13}}{(2J_k+1)\lambda^3} S_{\mathrm{M1}}, \text{ for M1 transition,}$$

$$A_{ki} = \frac{1.49097 \times 10^{13}}{(2J_k+1)\lambda^5} S_{\mathrm{M2}}, \text{ for M2 transition,}$$

where λ in units of Å represents the transition wavelength; k and i represent the higher and lower states of the transition, respectively; J_k is the total angular momentum quantum number of the higher state; S is the line strength of the M1 and M2 transitions. We used the biorthogonal transformation technique[32,33] to calculate line strengths, where the even and odd parity wavefunctions are built from independently optimized orbital sets.

The computational precision and accuracy are subject to the configuration space expanded by CSFs, i.e., the summation in Eq. (4). In this study, we adopted the same computational model described in Ref. [34]; hence, we have provided a sketch here. As a starting point, the Dirac–Hartree–Fock (DHF) calculation was carried out to optimize all occupied orbitals in the even and odd reference configurations. The even and odd reference configurations are $1s^22s^22p^63s^23p^63d^{10}4s^24p^65s^2$ and $1s^22s^22p^63s^23p^63d^{10}4s^24p^65s5p$, respectively. Furthermore, the correlation orbitals up to $n = 12$ and $l = 4$ were produced, being adapted to the valence–valence (VV) and the primary part of core–valence (CV) correlation CSFs. The VV correlation CSFs were generated by single (S) and double (D) excitations of electrons from the $n = 5$ valence shell to certain correlation orbitals, and the main part of CV CSFs by single and restricted double excitations from the $n = 3$ and $n = 4$ core shells to those correlation orbitals. The restricted double excitation indicates that at most one-electron from the core shell can be excited at a time. The correlation orbital set was augmented layer by layer, and such a layer consists of orbitals with different spatial symmetries, i.e., $s, p, d, f, \ldots$. Once the correlation orbital set was formed, the remaining CV correlation related to the $n = 1$ and $n = 2$ core shells was captured in the subsequent RCI calculation based on the above CSF expansion, marked as the VV + CV model.

The core–core (CC) correlations in the $n = 4$ core shell, labeled as the CC4 model, were also considered in the RCI computation. In this step, the CSFs produced by SD excitations of electrons from the $n = 4$ shell to the correlation orbitals were added into the CV + VV model. Additionally, only the first five layers of correlation orbitals were used to control the number of CSFs due to the negligible contribution from the remaining correlation orbitals. The higher-order electron correlation effects among the $n = 4, 5$ shells were further estimated using the multireference (MR)-SD approach. The MR configurations consist of $\{4s^24p^65s^2;\ 4s^24p^65p^2;\ 4s^24p^54d5s5p\}$ and $\{4s^24p^65s5p;\ 4s^24p^64d5p;\ 4s^24p^65s6p;\ 4s^24p^65p6s;\ 4s^24p^64d6p\}$ for the ground and excited states, respectively. The configuration space was further expanded by SD-excitation CSFs generated from the occupied orbitals in the MR configurations to five layers of virtual orbitals, which is marked as MR-5. Finally, the Breit interaction was included based on the MR-5 model. In practice, the GRASP2018 package[35] was employed to perform calculations.

Table 1 presents the calculated excitation energies, line strengths, and the rates of the $^1S_0$–$^3P_2^o$ M2 and $^3P_1^o$–$^3P_2^o$ M1 transitions as functions of the computational models. The line strength and rate with Babushkin and Coulomb gauges of $^3P_1^o$–$^3P_2^o$ E2 tran-

sition were also shown to examine the quality of our calculation. Furthermore, the corresponding lifetimes of the $^3P_2^o$ metastable state, $\tau_k = \{\sum_i A_{ki}\}^{-1}$, were given for different computational models. The other available theoretical values for the excitation energies and transition rates are displayed for comparison. As presented in this table, the VV and CV correlations make dominant contributions to the parameters concerned. The $n = 4$ CC and higher-order correlations lead to better agreement between our results and others. The Breit interaction changes the rates by 1% and 5% for the M1 and M2 transitions. It is worth noting that the Breit interaction was neglected in the previous calculations, although its contribution is not large. The uncertainty of our calculation can be controlled at a low level by considering the higher-order electron correlation and Breit interaction.

Table 1. Excitation energies ΔE, line strengths S, rates A of the $^1S_0$–$^3P_2^o$ M2, $^3P_1^o$–$^3P_2^o$ M1, and $^3P_1^o$–$^3P_2^o$ E2 (B: Babushkin gauge; C: Coulomb gauge) transitions and lifetime of the $^3P_2^o$ metastable state in different computational models.

Model	$^1S_0$–$^3P_2^o$ M2			$^3P_1^o$–$^3P_2^o$ M1			$^3P_1^o$–$^3P_2^o$ E2				Lifetime
	ΔE (cm^{-1})	S (10^2a.u.)	A (10^{-5}/s)	ΔE (cm^{-1})	S (a.u.)	A (10^{-4}/s)	S_B (10^3 a.u.)	S_C (10^3 a.u.)	A_B (10^{-7}/s)	A_C (10^{-7}/s)	τ (s)
DHF	8822.26	4.65	0.741	366.33	2.50	6.63	1.51	0.835	2.23	1.23	1492
VV + CV	14952.38	4.87	10.9	403.56	2.50	8.85	1.31	1.24	3.13	2.96	1006
CC4	13157.14	4.94	5.81	396.67	2.50	8.41	1.47	0.953	3.22	1.99	1112
MR-5	15435.73	5.11	13.3	399.00	2.50	8.56	1.47	1.15	3.34	2.60	1011
+Breit	15457.11	5.11	13.4	392.52	2.50	8.15	1.47	1.15	3.06	3.40	1054
						Others					
Derevianko[20]			12.7			8.26			3		1048
Liu *et al.*[21]	14734.03		10.7	390.39		8.25			2.700		1071

Other physical effects neglected in this study, such as the high-frequency part of the Breit interaction and quantum electrodynamical corrections, are tiny for the Sr atom. For the calculated excitation energy of the $^1S_0$–$^3P_2^o$ M2 transition that differs from the NIST value[36] by 4%, we revised the transition rate by replacing our calculated excitation energy with the NIST value. The resulting value is $1.12 \times 10^{-4}\,s^{-1}$.

Furthermore, we considered three sources of errors to estimate the uncertainty of our calculation. As indicated above, the M1 and M2 transitions are the primary decay channels; therefore, we focus on estimating the uncertainty of these two transitions. According to the convergence trends, the uncertainties of the rate for the $^1S_0$–$^3P_2^o$ M2 transition and $^3P_1^o$–$^3P_2^o$ M1 transition are approximately 4% and 2%, respectively. The contribution of the CC correlation related to the $n = 3$ core shell was estimated to be 2% and 3% for the M2 and M1 transition rates based on the CC4 model, respectively. Figure 3 shows the contribution of various computational models on the M1 and M2 transition rates to evaluate the effects of the remaining electron correlations. The number in this figure denotes the computational models, i.e., 1, 2, and 3 for the VV + CV, CC4, and MR-5 models, respectively. As shown in this figure, the contribution decreases approximately in the power of 2 as the expansion of the configuration space. According to this relation, the contribution of the remaining electron correlations was evaluated to be smaller than that of the CC correlation related to the $n = 3$ core shell, i.e., less than 2% and 3% for the M1 and M2 transition rates, respectively. Furthermore, the uncertainties of excitation energies may change the M2 and M1 transition rates by approximately 20% and 2%, respectively. Thus, the final uncertainties are obtained to be 20% and 3% for the M2 and M1 transition rates, respectively, by considering the largest one of the above-mentioned sources. Considering different contributions of the two primary decay channels to the lifetime, the value is $\tau_{^3P_2^o} = 1079(54)\,s$ with an uncertainty ∼5% for the $^3P_2^o$ metastable state of ^{88}Sr.

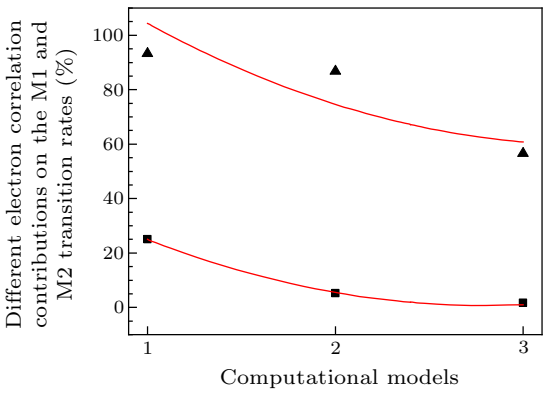

Fig. 3. The contributions from the electron correlations to the M1 and M2 transition rates as functions of the computational models. The numbers 1, 2, and 3 represent the VV + CV, CC4, and MR-5 models, respectively.

Figure 4 shows our measured and calculated $^3P_2^o$ metastable state lifetime and other available results. This figure shows that our theoretical result perfectly agrees with the previous calculations. Moreover, the theoretical values are consistent with our experimental measurement. Therefore, it can be understood that the updated BBR-induced decay rate resolved

the large discrepancy between the theoretical calculations and experimental measurements.

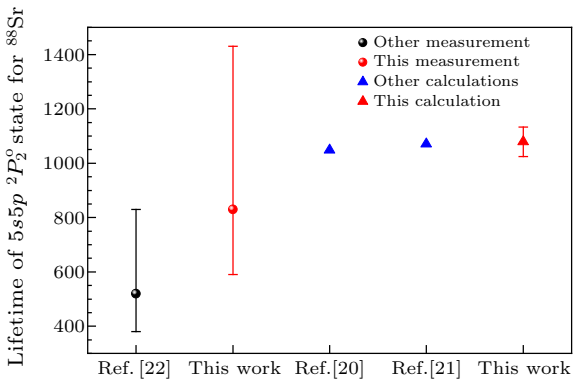

Fig. 4. A comparison of our determinations of the $5s5p\ ^3P_2^o$ metastable state lifetime and the other results available.

In summary, we have remeasured the lifetime of the $5s5p\ ^3P_2^o$ metastable state for ^{88}Sr. Our measurement is approximately 60% larger than the previous measurement.[22] We also obtain a more accurate value of the BBR-induced decay rate. Meanwhile, the metastable state lifetime was calculated using the MCDHF and RCI methods. In the calculation, we systematically considered the electron correlation effects in the active space approach and the Breit interaction. The theoretical result agrees with the previous calculations. We realize that the updated BBR-induced decay rate resolves the large discrepancy between theoretical and experimental determinations. With respect to the long lifetime of the $^3P_2^o$ state, it can be used in laser cooling and trapping experiments to further improve the stability of the optical lattice clocks.

Acknowledgments. This work was supported by the National Natural Science Foundation of China (Grant Nos. 11874090, 91536106, 61127901, 11404025, and U1530142), the Strategic Priority Research Program of CAS (Grant No. XDB21030100), the Key Research Project of Frontier Science of CAS (Grant No. QYZDB-SSW-JSC004), and the West Light Foundation of CAS (Grant No. XAB2018B17).

References

[1] Katori H, Ido T, Isoya Y and Kuwata-Gonokami M 2001 *AIP Conf. Proc.* **551** 382
[2] Grünert J and Hemmerich A 2002 *Phys. Rev. A* **65** 041401
[3] Yang C Y, Halder P, Appel O, Hansen D and Hemmerich A 2007 *Phys. Rev. A* **76** 033418
[4] Riedmann M, Kelkar H, Wübbena T, Pape A, Kulosa A, Zipfel K, Fim D, Rühmann S, Friebe J, Ertmer W and Rasel E 2012 *Phys. Rev. A* **86** 043416
[5] Sorrentino F, Ferrari G, Poli N, Drullinger R and Tino G M 2006 *Mod. Phys. Lett. B* **20** 1287
[6] Ushijima I, Takamoto M, Das M, Ohkubo T and Katori H 2015 *Nat. Photon.* **9** 185
[7] Falke S, Lemke N, Grebing C, Lipphardt B, Weyers S, Gerginov V, Huntemann N, Hagemann C, Al-Masoudi A, Häfner S, Vogt S, Sterr U and Lisdat C 2014 *New J. Phys.* **16** 073023
[8] McGrew W F, Zhang X, Fasano R J, Schäffer S A, Beloy K, Nicolodi D, Brown R C, Hinkley N, Milani G, Schioppo M, Yoon T H and Ludlow A D 2018 *Nature* **564** 87
[9] Oelker E, Hutson R B, Kennedy C J, Sonderhouse L, Bothwell T, Goban A, Kedar D, Sanner C, Robinson J M, Marti G E, Matei D G, Legero T, Giunta M, Holzwarth R, Riehle F, Sterr U and Ye J 2019 *Nat. Photon.* **13** 714
[10] Hill I R, Hobson R, Bowden W, Bridge E M, Donnellan S, Curtis E A and Gill P 2016 *J. Phys.: Conf. Ser.* **723** 012019
[11] Campbell S L, Hutson R B, Marti G E, Goban A, Darkwah O N, McNally R L, Sonderhouse L, Robinson J M, Zhang W, Bloom B J and Ye J 2017 *Science* **358** 90
[12] Häfner S, Falke S, Grebing C, Vogt S, Legero T, Merimaa M, Lisdat C and Sterr U 2015 *Opt. Lett.* **40** 2112
[13] Hashiguchi K, Akatsuka T, Ohmae N, Takamoto M and Katori H 2019 *Phys. Rev. A* **100** 042513
[14] Hobson R, Bowden W, Vianello A, Hill I R and Gill P 2020 *Phys. Rev. A* **101** 013420
[15] Yamaguchi A, Uetake S and Takahashi Y 2008 *Appl. Phys. B* **91** 57
[16] Yu D 2012 *Phys. Rev. A* **86** 032703
[17] Uetake S, Murakami R, Doyle J M and Takahashi Y 2012 *Phys. Rev. A* **86** 032712
[18] Bhongale S G, Mathey L, Zhao E, Yelin S F and Lemeshko M 2013 *Phys. Rev. Lett.* **110** 155301
[19] Daley A J, Boyd M M, Ye J and Zoller P 2008 *Phys. Rev. Lett.* **101** 170504
[20] Derevianko A 2001 *Phys. Rev. Lett.* **87** 023002
[21] Liu Y, Andersson M, Brage T, Zou Y and Hutton R 2007 *Phys. Rev. A* **75** 014502
[22] Yasuda M and Katori H 2004 *Phys. Rev. Lett.* **92** 153004
[23] Kelly J F, Harris M and Gallagher A 1988 *Phys. Rev. A* **37** 2354
[24] Wang Y B, Yin M J, Ren J, Xu Q F, Lu B Q, Han J X, Guo Y and Chang H 2018 *Chin. Phys. B* **27** 023701
[25] Safronova M S, Porsev S G, Safronova U I, Kozlov M G and Clark C W 2013 *Phys. Rev. A* **87** 012509
[26] Bjorkholm J E 1988 *Phys. Rev. A* **38** 1599
[27] Redondo C, Sánchez Rayo M N, Ecija P, Husain D and Castaño F 2004 *Chem. Phys. Lett.* **392** 116
[28] Nicholson T L, Campbell S L, Hutson R B, Marti G E, Bloom B J, McNally R L, Zhang W, Barrett M D, Safronova M S, Strouse G F, Tew W L and Ye J 2015 *Nat. Commun.* **6** 6896
[29] Grant I P 2007 *Relativistic Quantum Theory of Atoms and Molecules: Theory and Computation* (New York: Springer) p 518
[30] Fischer C F, Godefroid M, Brage T, Jönsson P and Gaigalas G 2016 *J. Phys. B* **49** 182004
[31] Johnson W R 2007 *Atomic Structure Theory-Lectures on Atomic Physics* (New York: Springer) p 185
[32] Olsen J, Godefroid M R, Jönsson P, Malmqvist P Å and Fischer C F 1995 *Phys. Rev. E* **52** 4499
[33] Verdebout S, Jönsson P, Gaigalas G, Godefroid M and Fischer C F 2010 *J. Phys. B: At. Mol. Opt. Phys.* **43** 074017
[34] Lu B, Zhang T, Chang H, Li J, Wu Y and Wang J 2019 *Phys. Rev. A* **100** 012504
[35] Fischer C F, Gaigalas G, Jönsson P and Bieroń J 2019 *Comput. Phys. Commun.* **237** 184
[36] Sansonetti J E and Nave G 2010 *J. Phys. Chem. Ref. Data* **39** 033103